ACS NANO

www.acsnano.org

ARTICLE

In Situ Raman and Fourier Transform Infrared Spectroscopy Studies of MXene–Electrolyte Interfaces

Tetiana Parker,[#] Yuan Zhang,[#] Kateryna Shevchuk,[#] Teng Zhang, Vikash Khokhar, Young-Hwan Kim, Givi Kadagishvili, David Bugallo, Manushree Tanwar, Ben Davis, Jongyoun Kim, Zahra Fakhraai,* Yong-Jie Hu,* De-en Jiang,* Dmitri V. Talapin,* and Yury Gogotsi*

Cite This: *ACS Nano* 2025, 19, 22228–22239

Read Online

ACCESS | Metrics & More | Article Recommendations | Supporting Information

ABSTRACT: **A comprehensive understanding of electrochemical interfaces is essential for the optimal performance of electrocatalysts, supercapacitors, and batteries. However, understanding the electrochemical behavior of MXenes during electrochemical processes by any single technique does not provide a whole picture. We achieved real-time monitoring in the complete near-mid-infrared chemical range by utilizing Raman spectroscopy (near-infrared (NIR) excitation) and Fourier transform infrared (FTIR) spectroscopy in the mid-infrared (MIR) range. The change of intramolecular O−H vibrations of MXene-confined water was monitored in real time using FTIR, while surface terminations were monitored by using Raman spectroscopy. The dynamic interplay between charge storage and the change in MXene surface chemistry was studied by employing representative electrolytes (0.5 M H_2SO_4, 1 M LiCl, and 6 M KOH) and comparing hydrophilic $Ti_3C_2T_x$ with mixed-terminations (T = O/OH/F) with hydrophobic chlorine-terminated $Ti_3C_2Cl_2$ MXene electrodes. *Ab initio* molecular dynamics (MD) simulations and density functional theory (DFT) calculations were used to shed light on ion insertion with a dynamic change of ion solvation and reveal the structure of the MXene-confined water.**

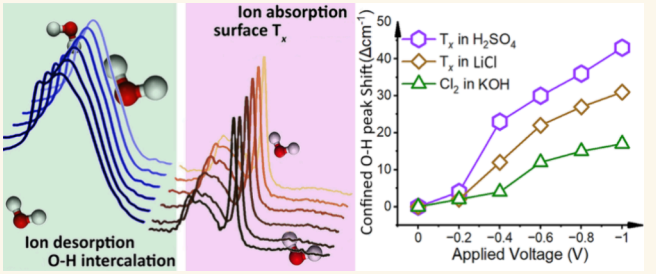

KEYWORDS: *MXene, electrochemical energy storage, in situ spectroscopy, Raman spectroscopy, Fourier transform infrared spectroscopy*

INTRODUCTION

Electrocatalysis and electrochemical energy storage have the potential to address the growing global energy demand and environmental concerns.[1] A deep understanding of the underlying electrochemical processes has been deemed imperative to optimize device performance. Traditionally, these processes have been analyzed *ex situ*,[2,3] which limited insights into real-time behavior due to a lack of understanding of the dynamic mechanisms. However, *in situ* techniques have recently been implemented to shed light on the electrochemical processes. For example, vibrational spectroscopies such as Fourier transform infrared (FTIR) and Raman spectroscopy have been employed to analyze the electrochemical reduction of graphene oxide films in organic solvents.[4] While these techniques are powerful individually, their combination provides complementary information, as FTIR probes change in dipole moment, whereas Raman tracks changes in polarizability. This distinction means that certain molecular vibrations will be selectively active in either Raman or FTIR spectroscopy. The synergistic use of both techniques offers a deeper understanding of novel two-dimensional (2D) material systems including MXenes.

MXenes, a novel class of 2D transition metal carbides, nitrides, and carbonitrides ($M_{n+1}X_nT_x$, where M is a transition metal, X is carbon or nitrogen, and T_x is surface termination (e.g., = −O, −F, −OH, and halogens)),[5] have emerged as promising materials for electrochemical applications due to their unique properties, including high conductivity,[6] tunable surface chemistry,[7] and large surface area.[8] MXenes have been explored as active materials in supercapacitors[9] and batteries,[10] wearable applications,[11] infrared (IR) shielding,[12] electromagnetic interference (EMI) shielding,[13] conductive binding additives,[14] and as current collectors.[15]

Received: March 3, 2025
Revised: May 20, 2025
Accepted: May 21, 2025
Published: June 9, 2025

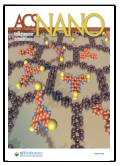

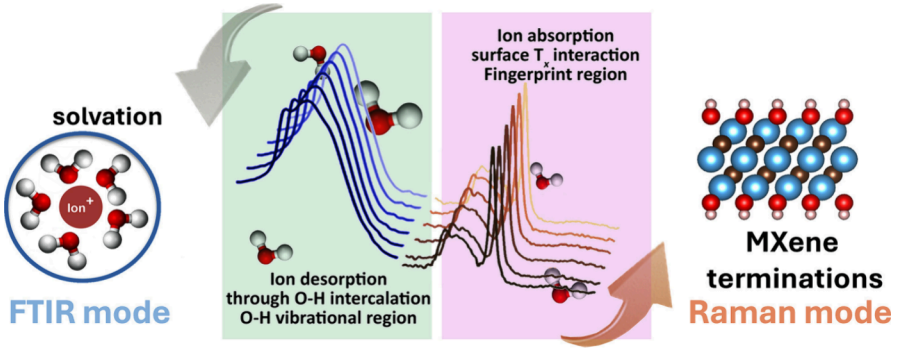

Figure 1. Concept of MXene *in situ* characterization. Combining FTIR and Raman spectroscopy enables comprehensive analysis of ion and MXene-confined water changes and an in-depth understanding of surface termination changes.

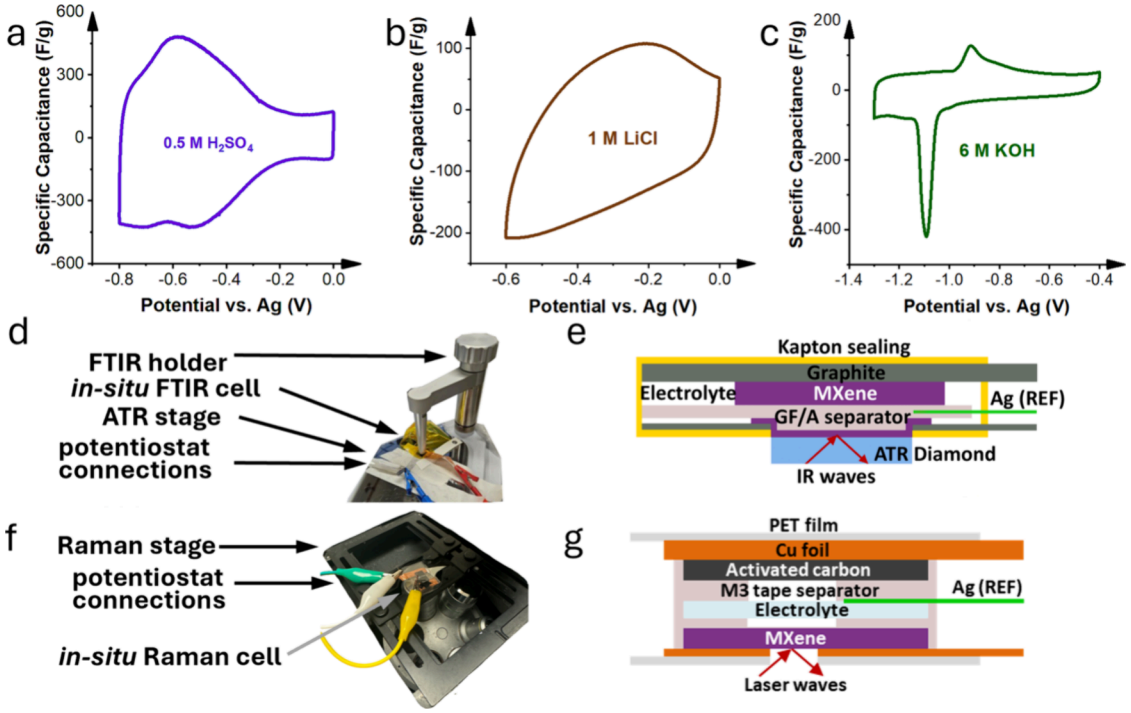

Figure 2. Concept of MXene electrochemical monitoring. (a) Cyclic voltammetry of $Ti_3C_2T_x$ in 0.5 M H_2SO_4, (b) cyclic voltammetry of $Ti_3C_2T_x$ in 1 M LiCl, (c) cyclic voltammetry of $Ti_3C_2Cl_2$ in 6 M KOH, (d) FTIR cell setup, (e) FTIR cell structure schematic (f) Raman cell setup, and (g) Raman cell structure schematic.

In situ studies of 2D materials, such as MXenes, have used specialized electrochemical cells. Confined cells, often employed with Raman spectroscopy, are constructed using materials such as glass or Kapton for cell encapsulation.[16] Integrated cells, frequently utilized with FTIR spectroscopy, are directly connected to the attenuated total reflectance (ATR) crystal.[7,17,18] Previous *in situ* studies with other 2D materials, such as graphene[4] and transition metal dichalcogenides,[19] have focused on tracking various changes. Chemical transformations, such as electrochemical hydrogen generation and storage,[20,21] and nitrogen (N_2) sorption in metal−organic frameworks (MOFs) have been investigated.[22] Catalytic reactions of the cobalt oxide catalyst[23] have also been monitored. *In situ* studies of MXenes have revealed crucial insights into their electrochemical behavior. Water evolution has been observed during various electrochemical reactions, such as intercalation and deintercalation of ions.[7,17] Many studies have also been focused on *in situ* characterization of structural[18] and optical changes[24] during electrochemical ion intercalation. However, the complex interplay among the MXene surface chemistry, structural evolution during ion intercalation, and solvent changes caused by ion desolvation during electrochemical reactions is yet to be better understood. To bridge this knowledge gap, this study introduces an *in situ* characterization approach combining Raman and FTIR spectroscopy to monitor the electrochemical behavior of MXenes in real time. By probing both NIR and MIR spectral regions, we have simultaneously tracked changes in intercalants and surface terminations during electrochemical cycling.

This study investigates the dynamic relationship between the charge storage and the adsorption of active species in aqueous electrolytes [sulfuric acid (0.5 M H_2SO_4), lithium chloride (1 M LiCl), and potassium hydroxide (6 M KOH)] with varying pH values. This research focuses on two types of MXenes: mixed-terminated $Ti_3C_2T_x$ and chlorine-terminated $Ti_3C_2Cl_2$. The primary goal is to understand how the hydrophilicity and hydrophobicity of the MXene surface affect charge storage and solvent dynamics in various aqueous electrolytes. FTIR

https://doi.org/10.1021/acsnano.5c03810
ACS Nano 2025, 19, 22228−22239

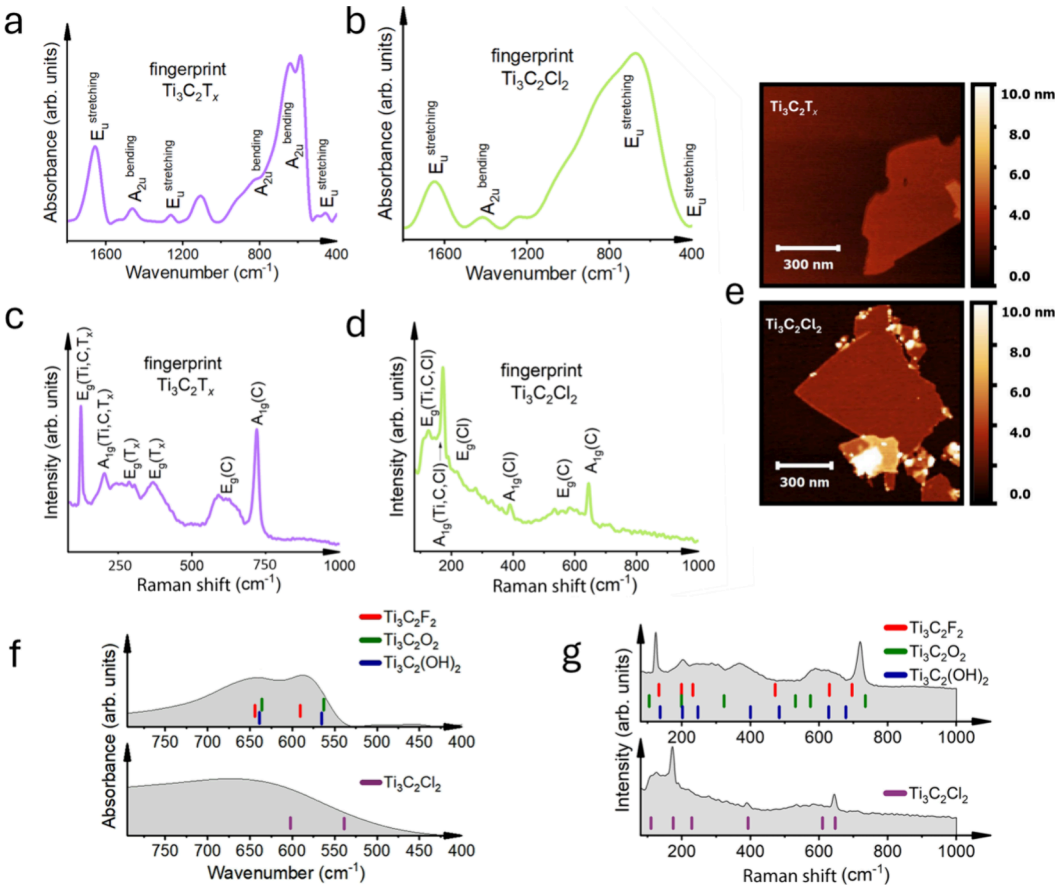

Figure 3. Chemical characterization of $Ti_3C_2T_x$ and $Ti_3C_2Cl_2$. (a) FTIR fingerprint of pristine $Ti_3C_2T_x$, (b) FTIR fingerprint of pristine $Ti_3C_2Cl_2$, (c) Raman fingerprint of pristine $Ti_3C_2T_x$, (d) Raman fingerprint of pristine $Ti_3C_2Cl_2$, (e) AFM images of $Ti_3C_2T_x$ (top) and $Ti_3C_2Cl_2$ (bottom) on the silicon substrate, (f) IR active vibrational peaks (bars represent DFT predicted IR vibrational peak positions, and gray areas represent experimental data of pristine $Ti_3C_2T_x$ and $Ti_3C_2Cl_2$), and (g) Raman active vibrational modes (bars represent DFT predicted Raman peak positions, and the gray areas represent experimental spectra of pristine $Ti_3C_2T_x$ and $Ti_3C_2Cl_2$).

spectroscopy is employed to analyze intramolecular vibrations, such as hydrogen bonding and O−H stretching vibrations in water. FTIR spectroscopy provides valuable insights into the strength and nature of hydrogen bonds, which are crucial for many electrochemical processes.[25] Raman spectroscopy is also utilized, as it is sensitive to changes in polarizability and effectively probes the vibrational modes of surface terminations, making it an ideal technique for studying MXene systems.[3,26]

To further study the underlying mechanisms, *ab initio* molecular dynamics (AIMD) simulations have been employed to investigate the behavior of confined water interacting with both ions and the MXene surface. Density functional perturbation theory (DFPT) calculations were performed on representative AIMD snapshots to obtain the change of vibrational signatures with the electrolytes and surface terminations of $Ti_3C_2T_x$ compared to those of $Ti_3C_2Cl_2$. AIMD, DFT, and DFPT results confirmed the experimental findings, providing a robust theoretical framework for interpreting the observed electrochemical phenomena. Additionally, atomic force microscopy (AFM) was used to study structural changes. Vibrational peak positions between selected $Ti_3C_2T_x$ and $Ti_3C_2Cl_2$ electrodes and vibrational fingerprints of $Ti_3C_2T_x$ compared to $Ti_3C_2Cl_2$ were recorded using both Raman and FTIR, providing a comprehensive analysis of electrode materials (Figure 1).

The study combines experimental and theoretical techniques to provide critical insights into the complex interfacial behavior of MXenes.[27] The insights will enable the rational design and optimization of high-performance, stable MXene-based electrochemical devices, paving the way for a sustainable energy future.

RESULTS AND DISCUSSION

***In Situ* Electrochemical Measurements.** To comprehensively investigate the electrochemical behavior of MXenes, three conventional electrode−electrolyte systems were chosen, which were characterized by fundamentally different chemistries. The systems selected include $Ti_3C_2T_x$ in 0.5 M H_2SO_4, $Ti_3C_2T_x$ in 1 M LiCl, and $Ti_3C_2Cl_2$ in 6 M KOH, exhibiting acidic and basic electrolytes and mixed and chlorine terminations on the MXene surface, respectively. While exploring all six possible combinations of two MXene types and three electrolytes that would provide a more exhaustive data set, this study focused on demonstrating *in situ* tracking of the most representative electrode−electrolyte pairs to illustrate key electrochemical behaviors. Future work will benefit from broader parametric studies; however, the present work prioritizes showcasing significant differences using representative members of the electrode−electrolyte pairs. Before *in situ* spectroscopic analysis, cyclic voltammetry (CV) was performed (Figure 2a−c) on each system to evaluate the

https://doi.org/10.1021/acsnano.5c03810
ACS Nano 2025, 19, 22228−22239

electrochemical stability and potential-dependent behavior of the MXene electrodes.

The CV curves revealed significant variations across the different electrolyte systems, highlighting the strong influence of the electrolyte on the electrochemical response of the MXenes. $Ti_3C_2T_x$ in H_2SO_4 displayed a pseudocapacitive curve with prominent redox peaks (Figure 2a). The redox peaks, observed at −0.6 V vs Ag, are attributed to reversible proton surface termination reactions occurring on the MXene surface.[28] In contrast, $Ti_3C_2T_x$ in LiCl exhibited characteristic capacitive behavior, consistent with previous reports in the literature (Figure 2b).[29] The most intriguing observation was the behavior of $Ti_3C_2Cl_2$ in 6 M KOH (Figure 2c). This system exhibited a pair of sharp peaks at −0.9 and −1.1 V, a phenomenon not previously reported for $Ti_3C_2Cl_2$ or other MXenes in the base electrolytes. The unique electrochemical response suggests a distinct charge storage mechanism in the system, likely influenced by the more hydrophobic surface of $Ti_3C_2Cl_2$ compared to that of $Ti_3C_2T_x$. To understand the charge storage mechanism within this system, both surface chemistry and changes in intercalants should be analyzed.

For *in situ* FTIR measurements (Figure 2d,e), the MXene working electrode was positioned directly onto an ATR crystal, ensuring efficient infrared light transmission and maximizing the interaction between the incident infrared beam and the MXene film. For optimal signal quality, Kapton encapsulation of the cell and a sample holder were employed to apply gentle pressure to the cell and maintain consistent contact between the MXene film and the ATR crystal.[2,7,17,18] For *in situ* Raman spectroscopic analysis (Figure 2f,g), the electrochemical cell was confined within transparent polyethylene terephthalate (PET) films. A hole was punctured at the measurement site to provide an unobstructed Raman signal collection while maintaining a controlled electrochemical environment.[30]

Both FTIR and Raman *in situ* cells presented here are characterized by their simplicity and affordability. Moreover, versatile cell designs can be easily adapted to accommodate various experimental conditions. The setup flexibility allows investigation of a wide range of electrochemical systems, making the *in situ* technique readily accessible and efficient for a broad spectrum of data measurements.

Chemical Characterization. A multifaceted approach was employed to delve into the chemical and structural properties of synthesized $Ti_3C_2T_x$ and $Ti_3C_2Cl_2$ MXenes. This involved the utilization of FTIR spectroscopy, Raman spectroscopy, and AFM. Additionally, DFT calculations were used to predict and validate the fingerprint region of the MXenes, providing a comprehensive understanding of their molecular structure and vibrational properties.

FTIR spectroscopy provides valuable insights into the vibrational modes of $Ti_3C_2T_x$ (Figure 3a) and $Ti_3C_2Cl_2$ (Figure 3b) MXenes, offering clues about their chemical composition and structural properties. The $Ti_3C_2T_x$ MXene, with its diverse surface terminations (=O, −F, and −OH), exhibited a prominent A_{2u} bending mode in the 600−400 cm^{-1} region. This spectral signature is characteristic of the =O, −F, and −OH functional groups (Tables S1,[2] S2,[2] S3). In contrast, the Cl-terminated $Ti_3C_2Cl_2$ MXene displayed a more pronounced E_u stretching mode in the 800−600 cm^{-1} region, confirming the dominance of −Cl terminations on its surface (Table S4). Raman spectroscopy further complemented the FTIR analysis by providing insights into the vibrational modes of the $Ti_3C_2T_x$ (Figure 3c) and $Ti_3C_2Cl_2$ (Figure 3d) MXene samples. The Raman spectrum of $Ti_3C_2T_x$ (Figure 3c) aligns with previously reported results, exhibiting three distinct regions: low-frequency vibrations of the whole flake, followed by vibrational modes from mixed surface terminations, and higher frequency vibrations dominated by carbon atoms.[26] The combination of in-plane and out-of-plane modes from heterogeneously distributed =O, −F, and −OH groups results in peak broadening, which was previously confirmed by MD simulations.[31] Therefore, it is unsurprising that Ti_3C_2 MXene, with homogeneously distributed chlorine terminations, shows three narrow bands (Table S4 and Figure 3d). They correspond to out-of-plane vibrations: the first peak at 173 cm^{-1} belongs to A_{1g} (Ti, C, Cl), while the 390 and 645 cm^{-1} peaks are related to the A_{1g} (Cl) and A_{1g} (C) modes, respectively. Additionally, the intensity of the peaks depends on the excitation wavelength,[32] which was maintained at 785 nm in all experiments to ensure consistency.

AFM analysis revealed some morphological differences between the MXene samples (Figure 3e). The single-layer MXene flake heights on the Si substrate, calculated from height distribution images as shown in Figure S5, are similar: 2.2 ± 0.3 nm for $Ti_3C_2T_x$ and 2.1 ± 0.2 nm for $Ti_3C_2Cl_2$. $Ti_3C_2Cl_2$ flakes had a more pronounced tendency to form larger, aggregated structures, as seen, for example, as brighter regions in the lower portion of the image. This stacking of multiple MXene flakes affects the overall morphology and uniformity. This disparity can be attributed to either stronger interlayer interactions in the Cl-terminated MXene or inefficient delamination. These morphological differences can potentially impact some applications, influencing factors such as electrical conductivity,[6] surface area,[8] and ion diffusion rates.[1] $Ti_3C_2T_x$ synthesis has been extensively optimized,[33] and further optimization for $Ti_3C_2Cl_2$ can potentially improve the single flake morphology, which is beyond this manuscript. In addition, some small white dots are also observed in $Ti_3C_2Cl_2$, which may be TiO_2 nanoparticles, salt,[34] or impurities resulting from the delamination process. However, we note that TiO_2 was not observed in the FTIR spectra. These flake heights are comparable to the previously reported $Ti_3C_2T_x$ flake height of 1.7 ± 0.1 nm measured from the substrate.[34]

DFT calculations were performed to better understand the observed experimental results and simulate the vibrational spectra of both $Ti_3C_2T_x$ and $Ti_3C_2Cl_2$, predicting the IR (Figure 3f) and Raman active (Figure 3g) vibrations. For $Ti_3C_2T_x$, various termination models (=O, −F, and −OH) were considered (Tables S1,[2] S2,[2] S3), while for $Ti_3C_2Cl_2$, a pure Cl-terminated model (Table S4) was selected. The calculated vibrational frequencies and intensities for IR and Raman spectra agreed with the experimental data (Figure 3f,g). The broad experimental spectra result from numerous peaks of mixed terminations, as predicted for $Ti_3C_2T_x$. In Figure 3f, DFT predictions indicate the presence of peaks at approximately 600 and 540 cm^{-1} for $Ti_3C_2Cl_2$, which are not sharply resolved in the experimental data. DFT predictions estimate singular vibration positions from idealized models, unlike experimental IR profiles, which accumulate intensities across a broad range. This results in a broader experimental spectral profile due to multiatom interactions. A broad peak observed in the experimental $Ti_3C_2Cl_2$ fingerprint region confirms this expected broadening. By combination of FTIR and Raman spectroscopy, a more comprehensive understanding of the vibrational properties of MXenes can be gained, aiding in the

https://doi.org/10.1021/acsnano.5c03810
ACS Nano 2025, 19, 22228−22239

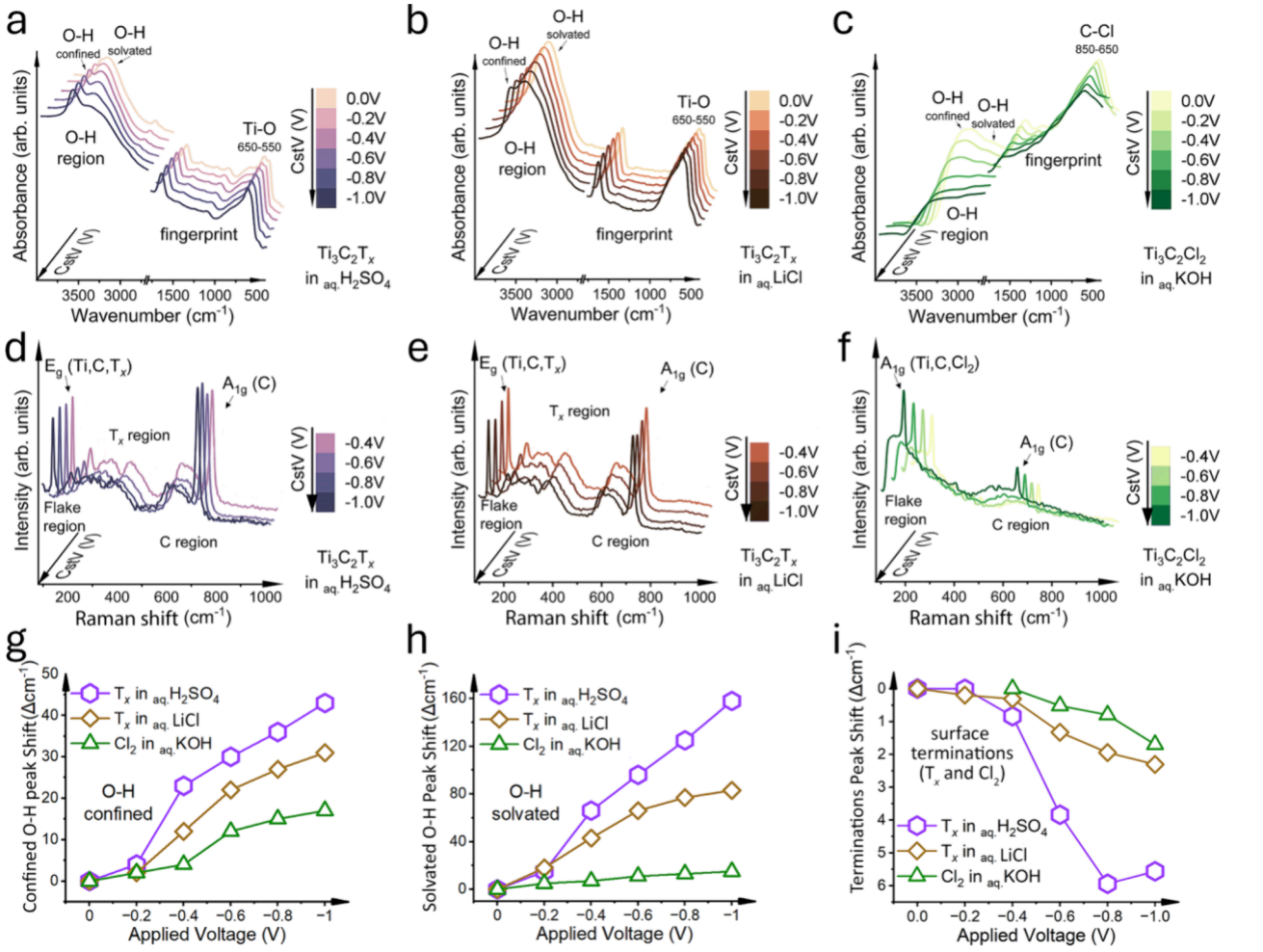

Figure 4. ***In situ*** **near-mid-infrared characterization. (a) FTIR spectra of $Ti_3C_2T_x$ in 0.5 M H_2SO_4, (b) FTIR spectra of $Ti_3C_2T_x$ in 1 M LiCl, (c) FTIR spectra of $Ti_3C_2Cl_2$ in 6 M KOH, (d) Raman spectra of $Ti_3C_2T_x$ in 0.5 M H_2SO_4, (e) Raman of $Ti_3C_2T_x$ in 1 M LiCl, (f) Raman spectra of $Ti_3C_2Cl_2$ in 6 M KOH, (g) confined vibrational peak shift, (h) O−H solvated vibrational peak shift, and (i) termination vibrational peak shift. Given the smaller magnitude of Raman shifts, panels (d−f) illustrate the electrochemical behavior from −0.4 to −1.0 V, where the most significant changes in the material's structure and composition are caused by electrochemical redox and ion intercalation processes (see panel (i)).**

optimization of their synthesis and applications in various fields.

In Situ **Spectroscopy.** To systematically investigate the impact of electrochemical potential on the chemical properties of MXene systems, a constant voltage holding (CstV) protocol was employed (Figure S1). The protocol involved a stepwise increase in voltage with a 2 min hold at each step for FTIR and Raman spectra recording. Applying the controlled potential bias induced specific electrochemical charge storage states in the MXene electrodes, enabling the study of the resulting chemical transformations. The approach allowed for a detailed examination of the relationship among applied potential, surface chemistry, and the overall electrochemical behavior of the MXenes.

FTIR spectroscopy (Figure 4a) revealed significant changes in the intramolecular vibrational region of the O−H[17] stretching (3700−2800 cm^{-1}) during the CstV experiment, particularly for the H_2SO_4 electrolyte. The changes are attributed to the dynamic interplay between weak charge-induced O−H stretching, which is water attracted by MXene surface oxygen terminations (in the frequency range of 3700−3500 cm^{-1} in the case of T_x and 3600−3200 in the case of Cl_2 terminations), and stronger cation-induced O−H stretching, that is, the water molecules that surround the cations (in a vibrational frequency range of 3500−3200 cm^{-1} in the case of T_x and 3200−2800 in the case of Cl_2 terminations) within the MXene nanoconfinement. The intensity and positions of the O−H peaks were sensitive to the potential-induced charge-surface interaction (Figure 4g,h). Under negative potential, a stronger interaction between the charge and the surface terminations was induced, which led to the redshift of both confined water peaks. In addition, the proton charge-induced O−H stretching peak intensity decreased with more negative potential, which implies the strengthening of the intermolecular hydrogen bonding network.[35] This indicates that the electrochemical state of MXene influences the hydrogen bonding network and the degree of water confinement. The above suggests that the electrolyte ions and applied potential can significantly affect the hydration environment and the interfacial properties of the MXene electrodes.

In the LiCl system, the behavior of confined and solvated O−H groups during the CstV experiment was also probed using *in situ* FTIR spectroscopy (Figure 4b). The O−H

https://doi.org/10.1021/acsnano.5c03810
ACS Nano 2025, 19, 22228−22239

stretching region exhibited distinct spectral features that evolved with the applied potential. The intensity and position of these peaks were sensitive to the degree of water confinement within the MXene interlayers (Figure 4g,h). The O−H stretching bands in the frequency range of 3700−3500 cm^{-1} associated with Li^+-confined water molecules dominated at lower potentials (0 V). As the potential increased (nearing −1 V), the intensity of these bands increased, while the intensity of bands associated with MXene-confined water molecules decreased. This suggests that the applied potential influences the distribution of water molecules within the MXene nanoconfinement. The redistribution of water molecules within the MXene confinement indicates ion desolvation, which can impact the ion transport properties and electrochemical performance of the MXenes.

Moreover, the Cl-terminated MXene (Figure 4c) exhibited a lower O−H band absorbance relative to that of the fingerprint region, suggesting the absence of hydroxyl groups on the surface. This observation aligns with the hydrophobic nature of the electrode.[32] This hydrophobicity can also be observed from the FTIR spectra in the water region (3600−2800 cm^{-1}). With the Cl-terminations, the accessibility of water molecules is greatly suppressed.[32] The difference in surface chemistry can significantly impact the interfacial properties of MXenes, influencing their electrochemical behavior and stability. Ti−O vibrations were observed in the 650−550 cm^{-1} region[2] for T_x-terminated $Ti_3C_2T_x$ systems immersed in both 0.5 M H_2SO_4 and 1 M LiCl electrolytes. Conversely, the C−Cl vibrations were detected in the 850−650 cm^{-1} region[36,37] for $Ti_3C_2Cl_2$ in 6 M KOH.

In situ Raman spectroscopy with 0.5 M H_2SO_4 revealed the most prominent changes in peak positions compared to those of other electrolyte systems (Figure 4d, Figure S6). The shifts of the in-plane E_g (Ti, C, T_x) mode (peak at 123 cm^{-1}) (Figure S6a,d) to higher wavenumbers and the out-of-plane A_{1g} (C) mode (peak at 720 cm^{-1}) (Figure S6h,k) to lower wavenumbers with decreasing potential were observed, confirming the protonation of the surfaces. In this case, peak shifts of 2 cm^{-1} (123.5 to 125.5 cm^{-1}) and 6 cm^{-1} (722 cm^{-1} to 716 cm^{-1}) were observed, and these shifts are reversible (Figure 4i). This phenomenon has been explored theoretically, showing that an abundance of OH surface terminations leads to the same peak changes we observed.[31] Additionally, previous *in situ* work by Johnson et al. described a similar 720 cm^{-1} peak position change in aqueous acidic electrolytes, whereas neutral electrolytes did not yield similar changes (in that study, the 123 cm^{-1} peak was not analyzed).[38] While this change has been attributed to proton absorption on the MXene surfaces, FTIR spectroscopy indicates that water, a weak Raman scatterer, interacts with MXene during electrochemical cycling, potentially leading to O−H bonds on the surfaces that produce Raman peak shifts.

Compared to the H_2SO_4 electrolyte, the MXene peak shift in 1 M LiCl is smaller (Figure 4e, Figure S6b,i). The in-plane vibrational mode of the entire flake shifted from 123.6 to 123.2 cm^{-1} (Figure S6f), and the out-of-plane carbon vibration shifted from 720.5 to 718.5 cm^{-1} (Figure S6m). While such small shifts could technically be attributed to a measurement error, the reversibility of these changes suggests their structural or compositional origin. Li^+-confined water molecules may interact with MXene surfaces, but due to the larger ion size, their contribution to surface terminations is less significant than in the sulfuric acid electrolyte. Additionally, a small shift (1.1 cm^{-1}) of the 720 cm^{-1} peak to the lower wavenumber has been previously reported in tensile stress experiments with 0.4% applied strain.[39] Therefore, the strain associated with insertion of ion into the structure may contribute to the observed peak shifts. This would also explain the shift of the 123 cm^{-1} peak to a lower wavenumber in the LiCl system. It contrasts with sulfuric acid, where the blue shift is indicative of increased O−H content, as shown by MD.[31] Together with FTIR spectroscopy, these findings suggest a large impact of ion−water molecule confinement in the system.

The electrochemical behavior of $Ti_3C_2Cl_2$ has not been previously studied *in situ*. We observed changes in the A_{1g} (C) vibrational mode with increasing potential in 6 M KOH (Figure 4f and Figure S6j). The smallest shift of 1.5 cm^{-1}, from 645.8 to 644.3 cm^{-1}, was noted (Figure 4i). Similar to the H_2SO_4 and LiCl systems, this shift may indicate a small contribution of ions to surface terminations. However, since the structure is uniformly terminated with chlorine and is highly stable, this shift is more likely to represent strain within the structure caused by the intercalation of large K^+ ions. As the contribution of water molecules is dampened in the FTIR spectra, it can be concluded that the structure remains stable in terms of surface terminations during electrochemical cycling.

Combining FTIR and Raman spectroscopy enables a comprehensive understanding of the reaction mechanisms and interfacial processes occurring at the MXene electrode−electrolyte interface. FTIR spectroscopy highlights the intricate interplay of water molecules with the MXene surface, distinguishing between different water environments and providing insights into the hydration and ion desolvation processes. With its precision in tracking vibrational mode shifts, Raman spectroscopy offers direct evidence of structural changes within the MXene lattice, attributed to factors such as ion intercalation/deintercalation, protonation of the surface, and strain induced by ion insertion. This combined approach allows for a deeper understanding of the complex interplay among the electrolyte, the MXene surface, and the electrochemical reactions at the interface. FTIR spectroscopy characterizes the water environment, and Raman spectroscopy provides insights into the structural and chemical transformations within the MXene lattice itself.

Understanding O−H Behavior. *In situ* FTIR spectroscopy was coupled with AIMD simulations and DFPT calculations to investigate further the complex interplay among the MXene surface, electrolyte ions, and solvent molecules. AIMD simulations provide a detailed atomistic view of the interfacial processes, including ion adsorption, solvation, and hydrogen bonding. By comparing the experimental FTIR spectra with the calculated vibrational spectra from DFPT, insights into the structural and dynamical properties of the MXene−electrolyte interface can be gained. This integrated approach allows for identifying specific molecular interactions, quantifying the degree of ion adsorption, and predicting the impact of different electrolyte compositions on the electrochemical performance of MXenes.

The FTIR spectra revealed significant changes in the O−H stretching region (3600−3400 cm^{-1}) during the electrochemical cycling. These changes are attributed to the dynamic behavior of water molecules at the MXene-electrolyte interface, which is influenced by the applied potential and nature of the electrolyte ions. The intensity and position of the O−H bands can be correlated with the degree of water confinement between the MXene surfaces.

https://doi.org/10.1021/acsnano.5c03810
ACS Nano 2025, 19, 22228−22239

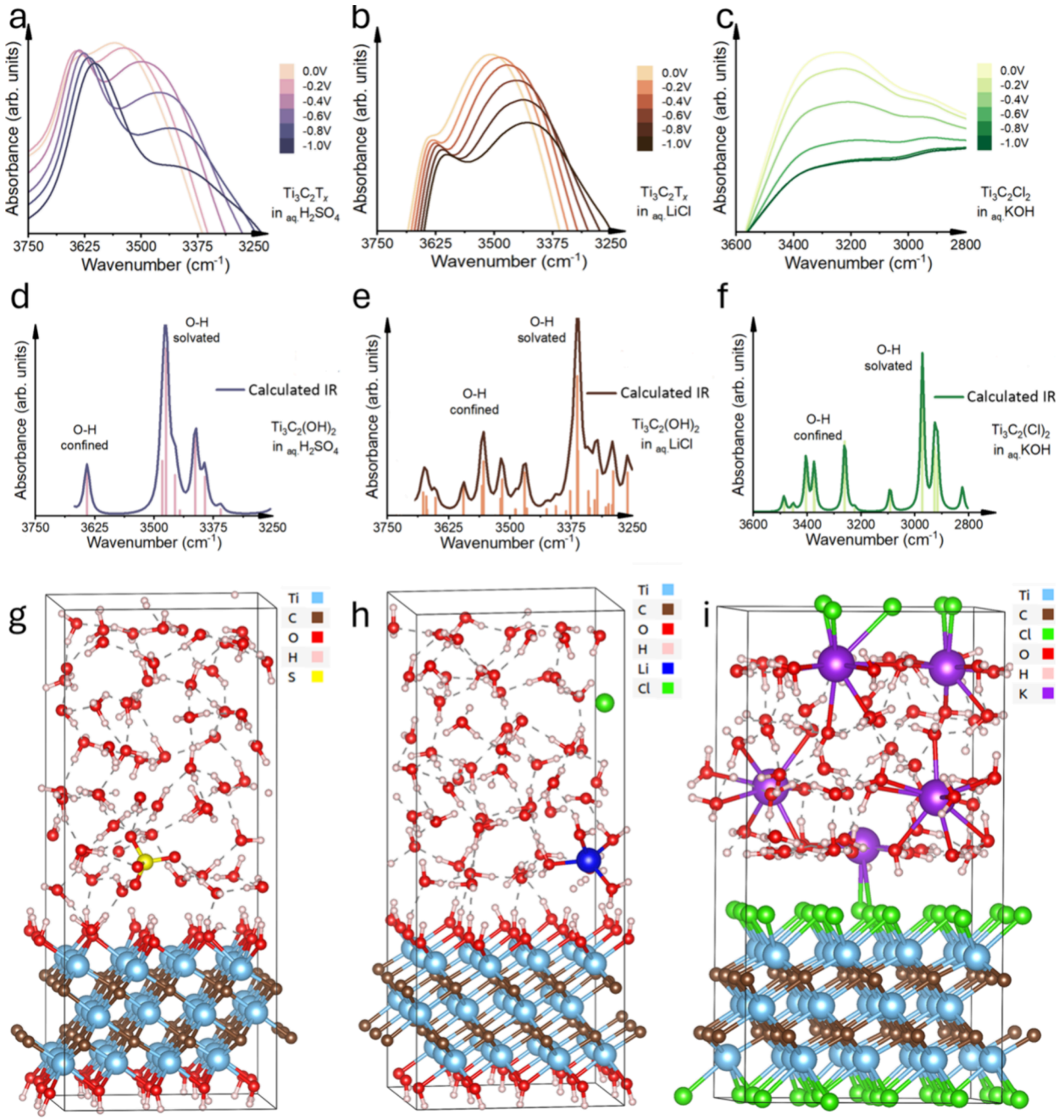

Figure 5. Signatures of the O−H stretching of MXene-confined water. (a) Experimental O−H region of $Ti_3C_2T_x$ in 0.5 M H_2SO_4, (b) experimental O−H region of $Ti_3C_2T_x$ in 1 M LiCl, (c) experimental O−H region of $Ti_3C_2Cl_2$ in 6 M KOH, (d) DFPT-calculated IR spectrum of the O−H region of $Ti_3C_2T_x$ in 1 M H_2SO_4, (e) DFPT-calculated IR spectrum of the O−H region of $Ti_3C_2T_x$ in 1 M LiCl, (f) DFPT-calculated IR spectrum of the O−H region of $Ti_3C_2Cl_2$ in 6 M KOH, (g) a snapshot of AIMD-simulated $Ti_3C_2T_x$ in 1 M H_2SO_4 at 5 ps, (h) a snapshot of AIMD-simulated of $Ti_3C_2T_x$ in 1 M LiCl at 5 ps, and (i) a snapshot of AIMD-simulated $Ti_3C_2Cl_2$ in 6 M KOH at 5 ps.

With increasing electrolyte pH, the intramolecular O−H stretching of MXene-confined water (3750−3500 cm^{-1}) shifts to a lower frequency region (Figure 5a−c), which indicates the weakening of the O−H bonding and stronger interaction between water molecules and MXene surface terminations.

Under negative potential, all of the peaks in the three systems shifted to a lower frequency range. For $Ti_3C_2T_x$ in the H_2SO_4 electrolyte, a pronounced peak shift to lower frequency is observed, which indicates that a stronger hydrogen bonding is induced under the nuclear quantum effect as more protons are transferred within the confinement.[35] In the LiCl electrolyte, the low-frequency peak shift is observed due to ion dehydration under applied potential that enhances the ion−water Coulombic force and weakens the O−H stretching vibration in water. For $Ti_3C_2Cl_2$ in the KOH electrolyte, with a weak hydrogen bonding network in the base electrolyte, the drastic intensity decrease in the peak at a lower frequency (3300−3200 cm^{-1}) shows a pronounced ion dehydration effect.

The AIMD snapshots in Figure 5g−i show the interactions between electrolyte ions, MXene layer, and water molecules, with solvation environments and hydrogen bonding. Figure S7 provides a detailed schematic illustrating the differences between solvated and confined −OH groups. The variations

https://doi.org/10.1021/acsnano.5c03810
ACS Nano 2025, 19, 22228−22239

in absorbance spectra between Figure 5d and e are attributed to the different electrolytes used, highlighting the electrolytes' influence on the water hydrogen-bond network and the interfacial behavior. Although such a difference can be already seen to some extent in the snapshots (Figure 5g,h), more in-depth computational modeling and analysis could shed further light in the future. For the present, this study aims to showcase the effectiveness of *in situ* FTIR and Raman spectroscopy as a primary analytical tool, with MD simulations providing supplementary insights. For the H_2SO_4 system (Figure 5a,d,g), the experimental and simulated spectra exhibited a strong peak at around 3625 cm^{-1}, corresponding to MXene-confined water molecules, and a broader peak at approximately 3500−3375 cm^{-1}, attributed to water molecules strongly hydrogen-bonded to the OH-terminated MXene surface. This suggests that the strong interaction with the protonated MXene surface leads to more strongly confined water layers at the MXene surface terminations. For the LiCl system (Figure 5b,e,h), the simulated spectra showed a more intense peak at around 3375 cm^{-1}, corresponding to more pronounced Li^+ charge-induced polarization of water molecules at the ion solvation shells, and a weaker peak at higher frequencies, indicating reduced MXene-confined water interaction. This observation is consistent with the weaker interaction between water and the MXene surface. In the case of the KOH system (Figure 5c,f,i), the simulated spectra revealed a strong and broad peak at a lower frequency range of around 3000 cm^{-1}, with the insignificant MXene-confined water peak, caused by the hydrophobicity of the Cl-termination.

CONCLUSIONS

This research, which combines *in situ* Raman and FTIR spectroscopy with DFT calculations and AIMD simulations, opens several important perspectives on the complex electrochemical behavior of MXenes, moving beyond a simple characterization of advanced energy materials. The real-time, near-mid-infrared monitoring enabled by this approach offers a unique window into the dynamic interplay between charge storage and MXene surface chemistry. Specifically, the simultaneous observation of changes in intramolecular O−H vibrations of MXene-confined water (using FTIR spectroscopy) and MXene surface terminations (using Raman spectroscopy) provides unprecedented insight into the behavior of water molecules at the MXene−electrolyte interface and the structural changes within the MXene lattice during electrochemical cycling. The ability to differentiate between hydrophilic and hydrophobic MXene terminations and to observe their distinct electrochemical responses in various electrolytes highlights the crucial role of surface chemistry in the MXene performance. Furthermore, the correlation of experimental data with computational modeling provides a robust framework for interpreting complex phenomena, revealing the intricate relationships among ion intercalation/deintercalation, protonation, strain, and water confinement within the MXene interlayers. The combined experimental and theoretical approach not only deepens the fundamental understanding of MXene interfacial behavior but also lays the groundwork for future investigations of tailored MXene materials for specific electrochemical applications. It offers a powerful methodology for exploring the intricacies of MXene electrochemistry and paves the way for the rational design of next-generation energy storage devices. The *in situ* tracking of interfacial dynamics, particularly the real-time observation of water molecules' behavior and MXene surface changes, offers a direct pathway to monitoring and optimizing electrolytes and selecting MXene surface terminations for enhanced charge storage. This detailed understanding of hydrophilic and hydrophobic MXene responses, coupled with our robust computational framework, enables precise tailoring of MXene, ultimately facilitating the development of next-generation energy storage devices with improved performance and stability.

EXPERIMENTAL SECTION

MXene Synthesis. $Ti_3C_2T_x$ and $Ti_3C_2Cl_2$ were synthesized to investigate their electrochemical properties and interfacial behavior. $Ti_3C_2T_x$ was synthesized via a conventional wet chemical etching method, employing a mixture of hydrofluoric acid (HF, $50_{aq.}$%, Sigma-Aldrich) and hydrochloric acid (HCl, $37_{aq.}$%, Sigma-Aldrich) as the etchant. The MAX phase precursor, Ti_3AlC_2,[6] was selected as the starting material for T_x and Cl-terminated MXenes. For T_x-terminated MXene preparation, the MAX phase was immersed in the etchant solution and subjected to a controlled temperature and time regimen.[6] The Al atoms were selectively etched, resulting in the exfoliation of the $Ti_3C_2T_x$ layers. Subsequent washing and centrifugation were employed to remove the residual etchant and impurities, yielding a multilayered $Ti_3C_2T_x$. It was delaminated using LiCl (99%, anhydrous, Sigma-Aldrich). In contrast, $Ti_3C_2Cl_2$ was synthesized through a molten salt etching of the same MAX phase.[40,41] The material preparation and etching were performed in an Ar-filled glovebox with oxygen and moisture levels below 1 ppm. The Ti_3AlC_2 MAX phase was mixed with $CdCl_2$ (99^+%, anhydrous, Strem) salt in a 1:8 molar ratio. The mixture was heated in an alumina crucible at 610 °C for 6 h. Cl-functionalized MXenes were recovered from the reaction mixture by dissolving excess $CdCl_2$ and Cd metal in concentrated aqueous HCl (12.1 M, 37%, fuming, Fisher), followed by washing with deionized water until neutral pH. The resulting MXene was dried under a vacuum at 45 °C for more than 12 h before further use.

AFM Characterization. AFM measurements were taken to compare the $Ti_3C_2Cl_2$ and $Ti_3C_2T_x$ MXene monolayers. The samples were prepared by spin coating (500 rpm for 60 s, 2000 rpm for 10 s). 100 μL of a dilute solution of each MXene was placed onto a Si wafer, which was cleaned for 10 min under oxygen plasma before spin coating. Afterward, a Bruker Icon AFM instrument was used to explore the surface in tapping mode. An AFM probe with a tip radius of ∼10 nm and a resonance frequency of ∼300 kHz (Tap300Al-G) was purchased from Budget Sensors Company. AFM images were acquired with a resolution of 512 samples per line. In the postanalysis, Gwyddion software was applied using the median of differences method to flatten the background. Height histograms shown in Figure S5 were generated after the flattening process and were used to calculate the flake thickness as the distance between the distribution of the substrate and that of the first flake. The full width at half-maximum for each distribution was used to estimate the error in thickness for each MXene.

DFT Modeling. Density functional theory (DFT) calculations within the Vienna *Ab initio* Simulation Package (VASP)[42] were employed to investigate the electronic and vibrational properties of MXenes. The projector-augmented wave (PAW)[43] method was utilized, and the Perdew−Burke−Ernzerhof (PBE)[42] generalized gradient approximation (GGA) function was adopted to describe electron exchange-correlation. A vacuum layer of approximately 10 Å was introduced to eliminate interactions between the 2D MXene slab and its periodic images. For the phonon calculations, the Brillouin zone was sampled by using a 6 × 6 × 1 Γ-centered k-point mesh, and a plane wave energy cutoff of 600 eV was employed. Phonon calculations were conducted by using density functional perturbation theory (DFPT) within a 4 × 4 × 1 supercell. The obtained phonon dispersion bands (Figure S2)[2] were corrected using the rotational sum rule,[43] and the infrared and Raman-active vibrational modes were predicted using the Phonopy Spectroscopy package.[44]

https://doi.org/10.1021/acsnano.5c03810
ACS Nano 2025, 19, 22228−22239

***In Situ* Spectroscopy Setup.** To enable real-time monitoring of the electrochemical processes at the MXene−electrolyte interface, a custom-built *in situ* electrochemical cell was designed to accommodate FTIR and Raman spectroscopy. A three-electrode setup with a silver (Ag) reference electrode was used in both cases. For *in situ* FTIR spectroscopy, a thin film of MXene was attached directly to the ATR crystal, which served as the working electrode. An oversized MXene film and Ag wire were applied as the counter and reference electrodes. A Whatman (GF/A) glass fiber membrane was used as a separator. The electrochemical cell was designed to minimize interference of cell components and ensure optimal optical alignment. An FTIR spectrometer (Bruker Invenio R) was employed to collect the vibrational spectra of the MXene electrode at various stages of the electrochemical cycle. Concave rubberband correction and 25-point average smoothing were applied to the FTIR spectra. The 2700−2000 cm^{-1} region was excluded from testing data as it only shows the ATR crystal signal.[2] *In situ* Raman spectroscopy was conducted using a Renishaw inverted inVia Raman spectrometer equipped with a 785 nm laser. A 63× objective lens (NA = 0.7), acquisition times of 30−60 s, and low laser powers were employed to prevent laser ablation. The *in situ* cell was assembled by placing a free-standing MXene film onto a PET film, followed by copper foils as the current collectors, a silver wire as the reference electrode, and an activated carbon counter electrode. The cell was sealed and insulated using 3M tape, with an electrolyte opening filled with filter paper during assembly. The electrolyte was introduced into the cell by using a syringe, and the assembled cell was secured on the Raman stage with tape. A Biologic SP-300 potentiostat was connected to each cell for electrochemical data recording simultaneously with FTIR and Raman spectra acquisition.

Electrochemical Testing. A Biologic SP-300 potentiostat was applied in this study. A constant voltage holding (CstV) protocol (Figure S1) induced specific electrochemical states in the MXene electrodes. The voltage was increased stepwise from 0 V to a predetermined value of −1 V vs Ag wire, with a fixed holding time of 2 min at each step of 0.2 V. This protocol allowed for a systematic investigation of the impact of electrochemical potential on the chemistry of MXenes and the aqueous solution confined between MXene nanosheets. During the CstV experiment, a constant potential was applied to the working electrode, while the current response was monitored over time. The electrochemical cell was held for enough time to stabilize the induced current, and the system could reach a steady state, enabling the *in situ* spectroscopic techniques to capture the chemical changes at the electrode−electrolyte interface.

AIMD Modeling. Density functional theory (DFT) calculations with the Vienna *Ab initio* Simulation Package (VASP) were performed for structure optimization.[45] PBE exchange-correlation functional and PAW pseudopotential were applied.[46−48] Plane-wave cutoff energy was 500 eV, and atomic positions were relaxed until a force convergence of 0.01 eV $Å^{-1}$. Grimme's DFT-D3 method was used for vdW corrections with zero-damping.[49] The Brillouin zone was sampled with a K-points grid 3 × 3 × 1 for surface calculation.[50] *Ab initio* molecular dynamics simulations (AIMD)[51] were performed with a Nosé−Hoover thermostat[52] in NVT ensemble, with a time-step of 1 fs and constant velocities at 300 K. AIMD equilibrated structures, at 300 K for 5 ps, were used for density functional perturbation theory (DFPT)[53] calculations to generate IR spectra using the code from Karhánek.[54]

12-unit supercell structures of $Ti_3C_2(OH)_2$ and $Ti_3C_2Cl_2$ were used as MXene surfaces. The −OH termination was chosen as $Ti_3C_2T_x$ representation because our previous AIMD simulations have shown that the −OH and -O terminations on the MXene surface are interconvertible via proton transfer with water,[55] while −F terminations are rather inert.[56] So, the $Ti_3C_2(OH)_2$ termination is a reasonable starting configuration, and future work will examine additional representations of the surface terminations. A random arrangement of water molecules and electrolyte ions was chosen on MXene surfaces with approximate concentrations of 1 M H_2SO_4 (Figure 5g), 1 M LiCl (Figure 5h), and 6 M KOH (Figure 5i) solutions, reasonably close to experimental values while saving computational cost. This resulted in three simulated systems (Figure 5, Figure S3): $Ti_3C_2(OH)_2$ + 1 M H_2SO_4, $Ti_3C_2(OH)_2$ + 1 M LiCl, and $Ti_3C_2Cl_2$ + 6 M KOH. Extensive equilibration and convergence checks were performed on the chosen initial configurations to validate its accuracy within the study's scope. As a test, three different initial structures were chosen for $Ti_3C_2(OH)_2$ in the 1 M LiCl model and the simulated radial distribution functions of Li^+-O_{water}, averaged over 3−5 ps, were similar (Figure S4), indicating that the water dynamics in these systems are fast enough for our AIMD simulations to reach equilibrium and sufficiently sample the configurations.

ASSOCIATED CONTENT

Data Availability Statement

The original data that support the findings of this study are available from the authors upon request.

Supporting Information

The Supporting Information is available free of charge at https://pubs.acs.org/doi/10.1021/acsnano.5c03810.

DFT vibrational positions; constant voltage holding (CstV) protocol; phonon dispersion bands; *ab initio* molecular dynamics simulations (AIMD) data; radial distribution functions of Li^+-O_{water}; atomic force microscopy (AFM) flake height distribution; Raman spectral peak position and intensity changes; comparison of OH-confined vs OH-solvated systems (PDF)

AUTHOR INFORMATION

Corresponding Authors

Zahra Fakhraai − *Department of Chemistry, University of Pennsylvania, Philadelphia, Pennsylvania 19104, United States;* orcid.org/0000-0002-0597-9882; Email: fakhraai@sas.upenn.edu

Yong-Jie Hu − *Department of Materials Science and Engineering, Drexel University, Philadelphia, Pennsylvania 19104, United States;* orcid.org/0000-0003-1500-4015; Email: yh593@drexel.edu

De-en Jiang − *Interdisciplinary Materials Science and Department of Chemical and Biomolecular Engineering and Department of Chemistry, Vanderbilt University, Nashville, Tennessee 37235, United States;* orcid.org/0000-0001-5167-0731; Email: de-en.jiang@vanderbilt.edu

Dmitri V. Talapin − *Department of Chemistry, The University of Chicago, Chicago, Illinois 60637, United States;* orcid.org/0000-0002-6414-8587; Email: dvtalapin@uchicago.edu

Yury Gogotsi − *A.J. Drexel Nanomaterials Institute and Department of Materials Science and Engineering, Drexel University, Philadelphia, Pennsylvania 19104, United States;* orcid.org/0000-0001-9423-4032; Email: gogotsi@drexel.edu

Authors

Tetiana Parker − *A.J. Drexel Nanomaterials Institute and Department of Materials Science and Engineering, Drexel University, Philadelphia, Pennsylvania 19104, United States;* orcid.org/0000-0001-5998-2617

Yuan Zhang − *A.J. Drexel Nanomaterials Institute and Department of Materials Science and Engineering, Drexel University, Philadelphia, Pennsylvania 19104, United States;* orcid.org/0000-0002-4083-0928

Kateryna Shevchuk − *A.J. Drexel Nanomaterials Institute and Department of Materials Science and Engineering, Drexel*

University, Philadelphia, Pennsylvania 19104, United States; orcid.org/0000-0001-7411-3110

Teng Zhang − *A.J. Drexel Nanomaterials Institute and Department of Materials Science and Engineering, Drexel University, Philadelphia, Pennsylvania 19104, United States;* orcid.org/0000-0002-4939-0594

Vikash Khokhar − *Interdisciplinary Materials Science, Vanderbilt University, Nashville, Tennessee 37235, United States;* orcid.org/0009-0009-1895-624X

Young-Hwan Kim − *Department of Chemistry, The University of Chicago, Chicago, Illinois 60637, United States;* orcid.org/0000-0003-0453-1434

Givi Kadagishvili − *Department of Chemistry, University of Pennsylvania, Philadelphia, Pennsylvania 19104, United States*

David Bugallo − *Department of Materials Science and Engineering, Drexel University, Philadelphia, Pennsylvania 19104, United States; CiQUS, Universidade de Santiago de Compostela, Santiago 15782, Spain;* orcid.org/0000-0002-5636-9267

Manushree Tanwar − *Department of Chemistry, University of Pennsylvania, Philadelphia, Pennsylvania 19104, United States;* orcid.org/0000-0002-7589-0496

Ben Davis − *A.J. Drexel Nanomaterials Institute and Department of Materials Science and Engineering, Drexel University, Philadelphia, Pennsylvania 19104, United States*

Jongyoun Kim − *A.J. Drexel Nanomaterials Institute and Department of Materials Science and Engineering, Drexel University, Philadelphia, Pennsylvania 19104, United States*

Complete contact information is available at: https://pubs.acs.org/10.1021/acsnano.5c03810

Author Contributions

#T.P., Y.Z., and K.S. contributed equally to the work. T.P. performed *in situ* FTIR analyses and DFT calculations. Y.Z. performed electrochemical measurements and supervised *in situ* FTIR and *in situ* Raman measurements. K.S. performed *in situ* Raman analyses and DFT calculations. T.Z. completed MAX phase synthesis and sample preparation for AFM measurements. V.K. performed MD calculations. Y.-H.K. synthesized $Ti_3C_2Cl_2$. G.K. performed AFM measurements. D.B. managed DFT calculations. M.T. managed AFM measurements. B.D. made significant intellectual contributions. J.K. made substantial editing and visual graphics contributions. Z.F. supervised AFM measurements. Y.-J.H. supervised DFT modeling. D.-e.J. supervised MD modeling. D.V.T. supervised $Ti_3C_2Cl_2$ synthesis. Y.G. supervised *in situ* Raman, *in situ* FTIR, electrochemical measurements, Ti_3AlC_2, and $Ti_3C_2T_x$ synthesis. The project was supervised through equal contributions from Z.F., Y.-J.H., D.-e.J., D.V.T., and Y.G. The manuscript was written with contributions from all authors.

Notes

The authors declare no competing financial interest.

ACKNOWLEDGMENTS

This work was supported by the U.S. National Science Foundation under grant CHE-2318105 (M-STAR CCI). DFT calculations were performed partially using the Picotte cluster at the Drexel University Research Computing Facility and partially using the Stampede2 cluster at TACC through allocation MAT220033 from the Advanced Cyberinfrastructure Coordination Ecosystem: Services & Support (ACCESS) program, which is supported by U.S. National Science Foundation Grants #2138259, #2138286, #2138307, #2137603, and #2138296. Y.Z. acknowledges financial support from the Alexander von Humboldt Foundation.

REFERENCES

(1) Simon, P.; Gogotsi, Y. Materials for Electrochemical Capacitors. *Nat. Mater.* **2008**, *7* (11), 845−854.

(2) Parker, T.; Zhang, D.; Bugallo, D.; Shevchuk, K.; Downes, M.; Valurouthu, G.; Inman, A.; Chacon, B.; Zhang, T.; Shuck, C. E.; Hu, Y.-J.; Gogotsi, Y. Fourier-Transform Infrared Spectral Library of MXenes. *Chem. Mater.* **2024**, *36* (17), 8437−8446.

(3) Shevchuk, K.; Sarycheva, A.; Shuck, C. E.; Gogotsi, Y. Raman Spectroscopy Characterization of 2D Carbide and Carbonitride MXenes. *Chem. Mater.* **2023**, *35* (19), 8239−8247.

(4) Viinikanoja, A.; Kauppila, J.; Damlin, P.; Suominen, M.; Kvarnström, C. *in situ* FTIR and Raman Spectroelectrochemical Characterization of Graphene Oxide upon Electrochemical Reduction in Organic Solvents. *Phys. Chem. Chem. Phys.* **2015**, *17* (18), 12115−12123.

(5) Naguib, M.; Kurtoglu, M.; Presser, V.; Lu, J.; Niu, J.; Heon, M.; Hultman, L.; Gogotsi, Y.; Barsoum, M. W. Two-Dimensional Nanocrystals: Two-Dimensional Nanocrystals Produced by Exfoliation of Ti_3AlC_2. *Adv. Mater.* **2011**, *23* (37), 4207−4207.

(6) Mathis, T. S.; Maleski, K.; Goad, A.; Sarycheva, A.; Anayee, M.; Foucher, A. C.; Hantanasirisakul, K.; Shuck, C. E.; Stach, E. A.; Gogotsi, Y. Modified MAX Phase Synthesis for Environmentally Stable and Highly Conductive Ti_3C_2 MXene. *ACS Nano* **2021**, *15* (4), 6420−6429.

(7) Lounasvuori, M.; Sun, Y.; Mathis, T. S.; Puskar, L.; Schade, U.; Jiang, D. E.; Gogotsi, Y.; Petit, T. Vibrational Signature of Hydrated Protons Confined in MXene Interlayers. *Nat. Commun.* **2023**, *14* (1), 1322.

(8) Li, X.; Huang, Z.; Shuck, C. E.; Liang, G.; Gogotsi, Y.; Zhi, C. MXene Chemistry, Electrochemistry and Energy Storage Applications. *Nat. Rev. Chem.* **2022**, *6* (6), 389−404.

(9) Yan, J.; Ren, C. E.; Maleski, K.; Hatter, C. B.; Anasori, B.; Urbankowski, P.; Sarycheva, A.; Gogotsi, Y. Flexible MXene/Graphene Films for Ultrafast Supercapacitors with Outstanding Volumetric Capacitance. *Adv. Funct. Mater.* **2017**, *27* (30), No. 1701264.

(10) Chen, C.; Xie, X.; Anasori, B.; Sarycheva, A.; Makaryan, T.; Zhao, M.; Urbankowski, P.; Miao, L.; Jiang, J.; Gogotsi, Y. MoS_2-on-MXene Heterostructures as Highly Reversible Anode Materials for Lithium-Ion Batteries. *Angew. Chem., Int. Ed.* **2018**, *57* (7), 1846−1850.

(11) Bi, L.; Perry, W.; Wang, R.; Lord, R.; Hryhorchuk, T.; Inman, A.; Gogotsi, O.; Balitskiy, V.; Zahorodna, V.; Baginskiy, I.; Vorotilo, S.; Gogotsi, Y. MXene Functionalized Kevlar Yarn *via* Automated, Continuous Dip Coating. *Adv. Funct. Mater.* **2024**, *34* (14), No. 2312434.

(12) Han, M.; Zhang, D.; Singh, A.; Hryhorchuk, T.; Eugene Shuck, C.; Zhang, T.; Bi, L.; McBride, B.; Shenoy, V. B.; Gogotsi, Y. Versatility of Infrared Properties of MXenes. *Mater. Today* **2023**, *64*, 31−39.

(13) Rakhmanov, R.; Shuck, C. E.; Al Hourani, J.; Ippolito, S.; Gogotsi, Y.; Friedman, G. Ultrathin MXene Film Interaction with Electromagnetic Radiation in the Microwave Range. *Appl. Phys. Lett.* **2023**, *123* (20), 204105.

(14) Malchik, F.; Shpigel, N.; Levi, M. D.; Penki, T. R.; Gavriel, B.; Bergman, G.; Turgeman, M.; Aurbach, D.; Gogotsi, Y. MXene Conductive Binder for Improving Performance of Sodium-Ion Anodes in Water-in-Salt Electrolyte. *Nano Energy* **2021**, *79*, No. 105433.

(15) Wang, C.-H.; Kurra, N.; Alhabeb, M.; Chang, J.-K.; Alshareef, H. N.; Gogotsi, Y. Titanium Carbide (MXene) as a Current Collector for Lithium-Ion Batteries. *ACS Omega* **2018**, *3* (10), 12489−12494.

(16) Wachs, I. E. *in situ* Raman Spectroscopy Studies of Catalysts. *Top. Catal.* **1999**, *8*, 57−63.
(17) Lounasvuori, M.; Zhang, T.; Gogotsi, Y.; Petit, T. Tuning the Microenvironment of Water Confined in $Ti_3C_2T_x$ MXene by Cation Intercalation. *J. Phys. Chem. C* **2024**, *128* (7), 2803−2813.
(18) Lounasvuori, M.; Mathis, T. S.; Gogotsi, Y.; Petit, T. Hydrogen-Bond Restructuring of Water-in-Salt Electrolyte Confined in $Ti_3C_2T_x$ MXene Monitored by Operando Infrared Spectroscopy. *J. Phys. Chem. Lett.* **2023**, *14* (6), 1578−1584.
(19) Yazdani, S.; Yarali, M.; Cha, J. J. Recent Progress on *in situ* Characterizations of Electrochemically Intercalated Transition Metal Dichalcogenides. *Nano Res.* **2019**, *12* (9), 2126−2139.
(20) Knözinger, H. *in situ* Raman Spectroscopy. A Powerful Tool for Studies in Selective Catalytic Oxidation. *Catal. Today* **1996**, *32* (1−4), 71−80.
(21) Pinilla-Sánchez, A.; Chávez-Angel, E.; Murcia-López, S.; Carretero, N. M.; Palardonio, S. M.; Xiao, P.; Rueda-García, D.; Sotomayor Torres, C. M.; Gómez-Romero, P.; Martorell, J.; Ros, C. Controlling the Electrochemical Hydrogen Generation and Storage in Graphene Oxide by *in situ* Raman Spectroscopy. *Carbon N Y* **2022**, *200*, 227−235.
(22) Embrechts, H.; Kriesten, M.; Hoffmann, K.; Peukert, W.; Hartmann, M.; Distaso, M. Elucidation of the Formation Mechanism of Metal−Organic Frameworks *via in situ* Raman and FTIR Spectroscopy under Solvothermal Conditions. *J. Phys. Chem. C* **2018**, *122* (23), 12267−12278.
(23) Chlebda, D. K.; Jodłowski, P. J.; Jędrzejczyk, R. J.; Łojewska, J. 2D-COS of *in situ* μ-Raman and *in situ* IR Spectra for Structure Evolution Characterisation of NEP-Deposited Cobalt Oxide Catalyst during n-Nonane Combustion. *Spectrochim. Acta A Mol. Biomol. Spectrosc.* **2017**, *186*, 44−51.
(24) Zhang, D.; Wang, R.; Wang, X.; Gogotsi, Y. *in situ* Monitoring Redox Processes in Energy Storage Using UV−Vis Spectroscopy. *Nat. Energy* **2023**, *8* (6), 567−576.
(25) Wang, Z.; Chen, J.; Li, Y.; Dong, K.; Yu, Y. EDL Structure of Ionic Liquid-MXene-Based Supercapacitor and Hydrogen Bond Role on the Interface: A Molecular Dynamics Simulation Investigation. *Phys. Chem. Chem. Phys.* **2022**, *24* (10), 5903−5913.
(26) Sarycheva, A.; Gogotsi, Y. Raman Spectroscopy Analysis of the Structure and Surface Chemistry of $Ti_3C_2T_x$ MXene. *Chem. Mater.* **2020**, *32* (8), 3480−3488.
(27) Gao, Q.; Sun, W.; Ilani-Kashkouli, P.; Tselev, A.; Kent, P. R. C.; Kabengi, N.; Naguib, M.; Alhabeb, M.; Tsai, W.-Y.; Baddorf, A. P.; Huang, J.; Jesse, S.; Gogotsi, Y.; Balke, N. Tracking Ion Intercalation into Layered Ti_3C_2 MXene Films across Length Scales. *Energy Environ. Sci.* **2020**, *13* (8), 2549−2558.
(28) Lukatskaya, M. R.; Kota, S.; Lin, Z.; Zhao, M.-Q.; Shpigel, N.; Levi, M. D.; Halim, J.; Taberna, P.-L.; Barsoum, M. W.; Simon, P.; Gogotsi, Y. Ultra-High-Rate Pseudocapacitive Energy Storage in Two-Dimensional Transition Metal Carbides. *Nat. Energy* **2017**, *2* (8), 17105.
(29) Wang, X.; Mathis, T. S.; Sun, Y.; Tsai, W.-Y.; Shpigel, N.; Shao, H.; Zhang, D.; Hantanasirisakul, K.; Malchik, F.; Balke, N.; Jiang, D.; Simon, P.; Gogotsi, Y. Titanium Carbide MXene Shows an Electrochemical Anomaly in Water-in-Salt Electrolytes. *ACS Nano* **2021**, *15* (9), 15274−15284.
(30) Li, L.; Xu, J.; Shi, M.; He, J.; Jiang, J.; Dai, K.; Jiang, Z.; Yan, C. *in situ* Raman Investigation and Application of MXene-Stabilized Polypyrrole Composite for Flexible Aqueous Batteries. *Mater. Des.* **2022**, *217*, No. 110606.
(31) Berger, E.; Lv, Z.-P.; Komsa, H.-P. Raman Spectra of 2D Titanium Carbide MXene from Machine-Learning Force Field Molecular Dynamics. *J. Mater. Chem. C Mater.* **2023**, *11* (4), 1311−1319.
(32) Zhang, T.; Shevchuk, K.; Wang, R. J.; Kim, H.; Hourani, J.; Gogotsi, Y. Delamination of Chlorine-Terminated MXene Produced Using Molten Salt Etching. *Chem. Mater.* **2024**, *36* (4), 1998−2006.
(33) Thakur, A.; Chandran, B. S. N.; Davidson, K.; Bedford, A.; Fang, H.; Im, Y.; Kanduri, V.; Wyatt, B. C.; Nemani, S. K.; Poliukhova, V.; Kumar, R.; Fakhraai, Z.; Anasori, B. Step-by-Step Guide for Synthesis and Delamination of $Ti_3C_2T_x$ MXene. *Small Methods* **2023**, *7* (8), No. 2300030.
(34) Fang, H.; Thakur, A.; Zahmatkeshsaredorahi, A.; Fang, Z.; Rad, V.; Shamsabadi, A. A.; Pereyra, C.; Soroush, M.; Rappe, A. M.; Xu, X. G.; Anasori, B.; Fakhraai, Z. Stabilizing $Ti_3C_2T_x$ MXene Flakes in Air by Removing Confined Water. *Proc. Natl. Acad. Sci. U. S. A.* **2024**, *121* (28), No. e2400084121.
(35) Flór, M.; Wilkins, D. M.; de la Puente, M.; Laage, D.; Cassone, G.; Hassanali, A.; Roke, S. Dissecting the Hydrogen Bond Network of Water: Charge Transfer and Nuclear Quantum Effects. *Science* **2024**, *386* (6726), No. eads4369.
(36) Tanabe, K.; Hayamizu, K.; Ono, S.; Wasada, N.; Someno, K.; Nonaka, S.; Inazumi, Y. Spectral Database System SDBS on PC with CD-ROM. *Anal. Sci.* **1991**, *7*, 711−712.
(37) *Infrared Spectroscopy Absorption Table*. LibreTexts. chem.libretexts.org/@go/page/22645.
(38) Johnson, D.; Hansen, K.; Yoo, R.; Djire, A. Elucidating the Charge Storage Mechanism on Ti_3C_2 MXene through *in situ* Raman Spectroelectrochemistry. *ChemElectroChem* **2022**, *9* (18), No. e202200555.
(39) Dong, M.; Hu, Y.; Zhang, H.; Bilotti, E.; Pugno, N.; Dunstan, D.; Papageorgiou, D. G. Micromechanics of $Ti_3C_2T_x$ MXene Reinforced Poly(Vinyl Alcohol) Nanocomposites. *Compos. C: Open Access* **2024**, *13*, No. 100427.
(40) Kamysbayev, V.; Filatov, A. S.; Hu, H.; Rui, X.; Lagunas, F.; Wang, D.; Klie, R. F.; Talapin, D. V. Covalent Surface Modifications and Superconductivity of Two-Dimensional Metal Carbide MXenes. *Science (1979)* **2020**, *369* (6506), 979−983.
(41) Jiang, M.; Wang, D.; Kim, Y.; Duan, C.; Talapin, D. V.; Zhou, C. Evolution of Surface Chemistry in Two-Dimensional MXenes: From Mixed to Tunable Uniform Terminations. *Angew. Chem.* **2024**, *136* (37), No. e202409480.
(42) Marquis, E.; Cutini, M.; Anasori, B.; Rosenkranz, A.; Righi, M. C. Nanoscale MXene Interlayer and Substrate Adhesion for Lubrication: A Density Functional Theory Study. *ACS Appl. Nano Mater.* **2022**, *5* (8), 10516−10527.
(43) Rems, E.; Anayee, M.; Fajardo, E.; Lord, R. L.; Bugallo, D.; Gogotsi, Y.; Hu, Y. Computationally Guided Synthesis of MXenes by Dry Selective Extraction. *Adv. Mater.* **2023**, *35* (45), No. 2305200.
(44) Skelton, J. M.; Burton, L. A.; Jackson, A. J.; Oba, F.; Parker, S. C.; Walsh, A. Lattice Dynamics of the Tin Sulphides SnS_2, SnS and Sn_2S_3: Vibrational Spectra and Thermal Transport. *Phys. Chem. Chem. Phys.* **2017**, *19* (19), 12452−12465.
(45) Kresse, G.; Furthmüller, J. Efficiency of *ab initio* Total Energy Calculations for Metals and Semiconductors Using a Plane-Wave Basis Set. *Comput. Mater. Sci.* **1996**, *6* (1), 15−50.
(46) Perdew, J. P.; Burke, K.; Ernzerhof, M. Generalized Gradient Approximation Made Simple. *Phys. Rev. Lett.* **1996**, *77* (18), 3865−3868.
(47) Blöchl, P. E. Projector Augmented-Wave Method. *Phys. Rev. B* **1994**, *50* (24), 17953−17979.
(48) Kresse, G.; Joubert, D. From Ultrasoft Pseudopotentials to the Projector Augmented-Wave Method. *Phys. Rev. B* **1999**, *59* (3), 1758−1775.
(49) Grimme, S.; Antony, J.; Ehrlich, S.; Krieg, H. A Consistent and Accurate *ab initio* Parametrization of Density Functional Dispersion Correction (DFT-D) for the 94 Elements H-Pu. *J. Chem. Phys.* **2010**, *132* (15), 154104.
(50) Monkhorst, H. J.; Pack, J. D. Special Points for Brillouin-Zone Integrations. *Phys. Rev. B* **1976**, *13* (12), 5188−5192.
(51) Iftimie, R.; Minary, P.; Tuckerman, M. E. *ab initio* Molecular Dynamics: Concepts, Recent Developments, and Future Trends. *Proc. Natl. Acad. Sci. U.S.* **2005**, *102* (19), 6654−6659.
(52) Nosé, S. A Unified Formulation of the Constant Temperature Molecular Dynamics Methods. *J. Chem. Phys.* **1984**, *81* (1), 511−519.
(53) Gajdoš, M.; Hummer, K.; Kresse, G.; Furthmüller, J.; Bechstedt, F. Linear Optical Properties in the Projector-Augmented Wave Methodology. *Phys. Rev. B* **2006**, *73* (4), No. 045112.

(54) Karhánek, D. *Dakarhanek: VASP-Infrared-Intensities*. Zenodo: **2020**.
(55) Sun, Y.; Zhan, C.; Kent, P. R. C.; Naguib, M.; Gogotsi, Y.; Jiang, D. Proton Redox and Transport in MXene-Confined Water. *ACS Appl. Mater. Interfaces* **2020**, *12* (1), 763−770.
(56) Song, H.; Jiang, D. First Principles Insights into Stability of Defected MXenes in Water. *Nanoscale* **2023**, *15* (39), 16010−16015.

https://doi.org/10.1021/acsnano.5c03810
ACS Nano 2025, 19, 22228−22239